Raytran: A Monte Carlo Ray-Tracing Model to Compute Light Scattering in Three-Dimensional Heterogeneous Media

Yves M. Govaerts and Michel M. Verstraete, *Member, IEEE*

***Abstract*— A model of radiation transfer in three-dimensional (3-D) heterogeneous media is designed and evaluated. This model implements state-of-the-art Monte Carlo ray-tracing techniques and is dedicated to the study of light propagation in terrestrial environments. It is designed as a *virtual laboratory*, where scenes of arbitrary complexity can be described explicitly and where the relevant radiative processes can be represented in great detail, at spatial scales relevant to simulate actual measurements. The approach capitalizes on the existing understanding of the elementary radiative processes and recognizes that the major difficulty in accurately describing the radiation field after its interaction with a typical terrestrial scene results from the complexity of the structure and the diversity of the properties of the elements of the scene. The output of the model can be customized to address various scientific investigations, including the determination of absorption profiles or of light-scattering distributions. The performance of the model is evaluated through detailed comparisons with laboratory measurements of an artificial target as well as with other established reflectance models for plant canopies.**

***Index Terms*—Canopy reflectance modeling, radiation transfer, light scattering, Monte Carlo, ray tracing.**

I. Introduction

SATELLITE remote sensing has proven useful in a wide variety of applications, from geophysics to city planning and from weather forecasting to environmental monitoring. Optical sensors operating in the spectral range of solar light (0.3–3 μm), in particular, have already contributed, albeit in largely empirical ways, to a better understanding of the nature and dynamical evolution of land cover and of its role in the climate system.

The full exploitation and the proper evaluation of existing and future spaceborne sensors require the development of high-performance tools and techniques to extract reliable and accurate information from the data gathered by these platforms. In turn, the quantitative interpretation of remote-sensing data must be based on a clear understanding of the radiative processes that control the measurements, at the spatial scales and resolutions sampled by the observing instrument. In the case of optical sensors observing land surfaces, the radiation received by the instrument may have interacted with one or more geophysical media, namely, the atmosphere (including the various gases, aerosols, and clouds it may contain), the vegetation canopy, when one is present, and the underlying surface (soil and rocks, lakes and rivers, snow and ice, etc).

The propagation of light and its interactions with material objects is fundamentally explained by quantum physics. However, for the purpose of remote-sensing-data interpretation, the relevant macroscopic processes are usefully described by the equation of radiation transfer. In this case, the nature of the interaction between the radiation and the medium is expressed in terms of statistical properties, such as the single-scattering albedo or the phase function. Historically, radiation transfer has been studied first in the context of large natural sources of light, such as stars, or for major applications, such as nuclear reactor simulations or climate investigations. Due to their sizes and to the crucial role of gravitation, stellar and planetary atmospheres are largely layered media, where the radiative properties of the medium vary much faster along the gravity gradient than in the "horizontal" plane. As a result, much effort has been made to develop one-dimensional (1-D) models of radiation transfer.

Terrestrial environments (both natural and human made) exhibit significant variability at a variety of spatial scales. They also evolve in time in complex ways. One-dimensional vertical models of radiation transfer have been successfully applied to the description of the broad patterns of light absorption and scattering in reasonably layered geophysical media, such as the atmosphere, soils, and fully developed vegetation canopies. Nevertheless, in many situations, the heterogeneity of the scene is such that the proper interpretation of the measurements requires more advanced models.

The first three-dimensional (3-D) models of radiation transfer, initially developed in the early 1980's, built on previous experience by considering complex media, such as vegetated environments as assemblages of cells, each treated individually as a turbid medium [1]. In parallel, advanced methods, such as the discrete ordinate approach, first developed in astrophysics [2], were applied to represent the transport of photons in plant canopies (e.g., [3]). Monte Carlo techniques and computer graphics methods, such as ray tracing and radiosity, have also been used to simulate the absorption and scattering of light by realistic scenes (e.g., [4]–[6]). Each of these various approaches has its own advantages and drawbacks, depending on the model objective, and their comparisons have been the subject of an abundance of literature [5], [7], [8].

Manuscript received June 7, 1996; revised December 9, 1997.

Y. M. Govaerts is with Eumetsat, D-64295 Darmstadt, Germany (e-mail: govaerts@eumetsat.de).

M. M. Verstraete is with Space Applications Institute, Joint Research Centre, I-21020 Ispra (VA), Italy (e-mail: michel.verstraete@jrc.it).

Publisher Item Identifier S 0196-2892(98)00551-8.

In this evolution, it appears that the focus of attention has shifted from the solution of progressively more complicated equations to the description of more and more complex scenes. Indeed, the radiative processes that control the interactions between the radiation field and the elements of the scene being observed by the instrument are relatively well known and can be studied further in the laboratory, if needed. The main difficulty, at this point, is to account for the very large number of individual interactions between the field of radiation and the elements constituting the scene of interest.

The following challenges delimit the state-of-the-art and indicate the main areas of research and development in this field,

1) In most cases of interest, the radiation actually received by the instrument has interacted with and, hence, carries information about, the properties of multiple geophysical media (e.g., atmosphere, vegetation, and soil). Since these media are often radiatively coupled, in the sense that multiple scattering between them prevents the simple decoupling of their respective effects on the observed radiation field, the models must represent the transfer of radiation in each of the relevant media as well as their interactions.
2) Even when the instantaneous field-of-view of the instrument is very limited, field, airborne, and spaceborne sensors often acquire data for rather heterogeneous targets, characterized by a variety of radiative properties. The models should, thus, be able to take the structure and diversity of the environment into account.
3) By shifting the focus from the solution of equations to the accurate representation of the scene of interest, much more demanding requirements are placed on the detailed description of the objects in the scene. For instance, the simulation of a plant canopy with a ray-tracing model requires detailed information on the structure and optical properties of all elements in the scene. This evolution has significant implications, in terms of the quality and quantity of data that need to be gathered in field studies or in the laboratory.

The Raytran model described in the following section represents a step forward in these directions. The Monte Carlo ray-tracing technique and its implementation in this model assumes that the application falls within the domain of applicability of geometric optics. This model is independent of scale, provided the size of the simulated objects is much larger than the wavelength of the radiation. The scene of interest can be described completely independently from the problem of radiation transfer, and the physics of the interactions between the radiation and the objects in the scene is described through the selection of appropriate physical mechanisms and the assignment of the corresponding optical properties of the objects.

II. Description of the Model

The description of radiation transfer within an arbitrary scene is achieved on a ray-by-ray basis by using Monte Carlo ray-tracing techniques, generating rays in the forward direction, i.e., from the energy source to the scene. This technique needs to be optimized to limit the number of rays required to achieve a given level of accuracy. Classical optimization methods are based on variance reduction techniques, which have been the subject of an abundance of literature (e.g., [9] and references therein). There is no unique optimal-sampling strategy, and the solution may depend on the nature of the problem [10]. When applied to radiative-transfer computation with ray-tracing methods, most commonly used optimization approaches are based on reverse ray tracing, where the rays are generated from the detectors to the scene. Such an approach may be adequate to generate synthetic images, but may not be able to account for all physical processes. Hence, we simulate ray propagation in a physically meaningful way, i.e., in the forward direction, without any weighting mechanism. As a consequence, the radiative-transfer computation is based on a straightforward Monte Carlo scheme. Since this approach is very computer intensive, the design of the code has been carefully optimized to take advantage of the latest hardware and software parallelization developments [11]. Indeed, Monte Carlo ray-tracing techniques provide a well-defined and well-adapted problem for parallel computing. The elements of the model are described next.

The radiation impinging on the scene is conceptualized as a set of N-rays interacting with a collection of M-geometrical objects $O_{l=1,\ldots,M}$ of arbitrary shape, location, size, and orientation. Scattering functions are assigned to each of these objects. The trajectory of each ray is tracked through the scene from interaction to interaction until the ray is absorbed or leaves the scene. When a ray-matter interaction occurs, the ray is scattered in one and only one direction, assuming elastic-scattering processes. Formally, a ray path L_k can be expressed as a sequence of k_Q-radiative events $q_{k_0} \rightarrow q_{k_1} \rightarrow \cdots \rightarrow q_{k_Q}$. Each event q_{k_j} is characterized by a set of information $q_{k_j} = \{P_j; \Omega_j; T_j; O_l\}_k$, where the index $_{k_j}$ indicates the interaction j of ray k; P_j is the origin of the ray; Ω_j is its direction; and T_j is the type of interaction (emission T^E, reflection T^R, transmission T^T, or absorption T^A). The position P_j of an interaction point is expressed in an absolute system of coordinates (also called the world coordinate system) (Fig. 1). The direction of propagation Ω_j is expressed in polar coordinates (θ_j, ϕ_j), with respect to the same coordinate system.

Basically, three main preliminary steps are necessary to set up an experiment with this model. The first one consists of creating the target with geometrical primitives and assigning an interaction model to each object. The description of the scene is therefore completely independent of computation of the ray trajectories. The energy sources from which the rays are generated need to be characterized next. Finally, we have to perform measurements by defining filters to extract relevant information from ray paths. The computation of the radiation transfer in the scene is itself composed of four main steps.

1) *Generation of the rays:* Rays are generated in the forward mode from one or more energy sources (see Section II-A).
2) *Localization of the ray-object intersection:* This step constitutes the main task of any ray tracer and is described in Section II-B.

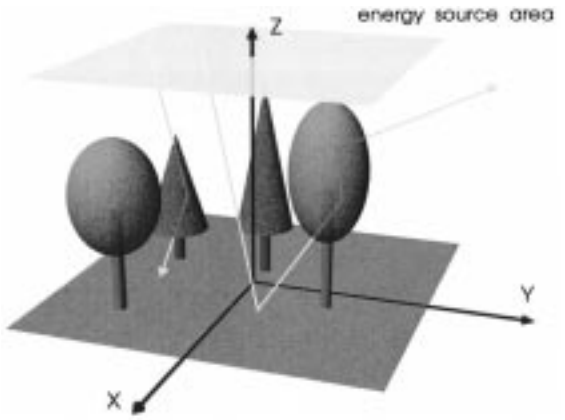

Fig. 1. Structural properties of the scene are described with geometrical primitives, whose location, orientation, and dimensions are given in a world Cartesian system. One or more energy sources may be located either inside or outside the scene.

3) *Determination of the type of interaction and the scattering direction:* When an interaction occurs, the type (absorption, reflection, transmission) is selected according to the probability-density function of the corresponding events. In case of scattering, the new direction is defined with a random variate distribution based on the interaction model (Section II-C).
4) *Extraction of relevant information from the ray paths:* This step, which consists of performing "virtual measurements" on the basis of the simulated radiative events, is described in Section II-D.

Steps 1)–4) are executed for all generated rays, while Steps 2) and 3) are repeated until rays are either absorbed or leave the outer boundary of the modeled scene.

A. Generation of the Rays

The emission of radiation is defined by W-different monochromatic energy sources located inside or outside the scene. Each energy source is defined by a plane area over which the origin of the rays P_0 is uniformly distributed and a number N_w of rays to be emitted with $N = \sum_{w=1}^{W} N_w$. The direction Ω_0 of an emitted ray is defined by the associated emissivity distribution function $\epsilon(\Omega)$. Different energy sources can be combined to simulate complex illumination conditions. In the case of natural lighting, the illumination is composed of direct radiation from the sun and scattered radiation by the atmosphere. Direct emissivity is simply simulated by a Dirac delta function $\epsilon(\Omega) = \delta(\Omega - \Omega_0)$, where Ω_0 is the direction of emission. Since Raytran is capable of modeling radiative transfer in turbid media, as will be seen in Section II-C, it is possible to simulate explicitly the atmospheric scattering and absorption effects, taking into account its vertical heterogeneity, the multiple interaction between the soil and the atmosphere, and the presence of clouds.

B. Localization of the Intersection Points

The generation of a meaningful scene represents one of the main tasks of the realization of an experiment. In principle, all targets of interest to environmental remote-sensing studies may be represented, i.e., from a single leaf [12] or needle up to a complete landscape. Since this model is based on geometrical optics theory, all individual objects in the scene must be larger than the wavelength of the simulated radiation. The objects $O_{l=1,\ldots,M}$ interacting with the radiation field are represented explicitly as 3-D geometrical structures. The geometrical primitives are characterized by their location, orientation, and dimension. Object positions are given, with respect to the world Cartesian coordinate system, as shown in Fig. 1. Primitives can be combined (union, difference, and intersection) to produce more complex objects with the Constructive Solid Geometry (CSG) technique [13]. Primitives may be classified into two categories: open or closed objects. Closed primitives (e.g., spheres, boxes, torus) enclose a portion of space for which "inside" can be clearly distinguished from the "outside" with a surface whose normal is pointing outward. By contrast, open objects are typically surfaces that do not define a bounded volume (e.g., discs, polygons, and cylinders).

Computing the point of intersection with the surface closest to a ray of origin P_j and direction Ω_j is the basic operation of the ray tracer. The intersection point P_{j+1} is searched for by using an optimized geometrical-sorting algorithm, based on the bounding of an individual or a list of objects in axis-aligned bounding boxes or by a uniform subdivision of part of the scene in smaller volumes called "voxels" [14]. If the ray does not intersect any object, it leaves the scene and contributes to the computation of the overall reflectance of the scene.

C. Ray-Object Interaction

When a ray collides with an object of the scene, its trajectory is affected by the optical properties of that object. It is therefore necessary to model, in the context of geometrical optics, how rays interact with the material objects represented in the model. We shall always assume that a reflected or transmitted ray has the same energy (wavelength) as the incident one, such that a ray is either completely absorbed or reemitted. The interaction models should provide the type of interaction or scattering event (reflection, transmission, or absorption) and the outgoing direction Ω_{j+1} on the basis of the knowledge of the characterization of incident ray direction Ω_j, intersection point coordinates P_{j+1}, and the outgoing surface normal at that point Ω_L.

In Raytran, rays are always traveling in media that may be absorbing and scattering. A medium, defined as an elementary radiative unit, is a geometrical object characterized by its position, its spatial extension, and its interaction model. It may contain other objects with different optical properties. Interaction models characterize the scattering process at the interface between two media as well as the propagation in the medium. Infinitely thin media may also be defined with open objects. They are considered a degenerate case in which the interaction at the interface is the only one defined. This kind of medium is useful for describing plant leaves in the context of a full canopy for instance.

1) Interaction at the Interface Between Two Media: When a light pencil falls onto a boundary between two homogeneous media of different optical properties, it is split into

a transmitted wave proceeding in the second medium and a reflected wave propagated back into the first medium. Let us consider the case of a ray intersecting an open surface or the envelope delimiting a scattering homogeneous medium. Conceptually, the type of interaction with that surface is defined first, then the outgoing direction is specified. The scattering direction is computed in the coordinate system local to the point of intersection, such that the normal to the surface is the vector $(0, 0, 1)$. Hence, directions expressed in this coordinate system are noted with a $'$. Surface properties are typically characterized by the probabilities that a ray coming from direction $\Omega'_j(\theta'_j, \phi'_j)$ is reflected

$$\rho_p(\theta'_j, \phi'_j) = \int_0^{2\pi} \int_0^{\pi/2} \rho(\theta'_j, \phi'_j; \theta'_{j+1}, \phi'_{j+1}) \cdot \sin\theta'_{j+1} d\theta'_{j+1} d\phi'_{j+1} \quad (1)$$

transmitted

$$\tau_p(\theta'_j, \phi'_j) = \int_0^{2\pi} \int_{-\pi/2}^{0} \tau(\theta'_j, \phi'_j; \theta'_{j+1}, \phi'_{j+1}) \cdot \sin\theta'_{j+1} d\theta'_{j+1} d\phi'_{j+1} \quad (2)$$

or absorbed

$$\alpha_p(\theta'_j, \phi'_j) = 1 - \rho_p(\theta'_j, \phi'_j) - \tau_p(\theta'_j, \phi'_j). \quad (3)$$

Only two probability-density functions need to be defined to describe the surface properties. $\rho(\theta'_j, \phi'_j; \theta'_{j+1}, \phi'_{j+1})$ and $\tau(\theta'_j, \phi'_j; \theta'_{j+1}, \phi'_{j+1})$ are called the bidirectional reflectance and transmittance functions, respectively. The function ρ describes the conditional probability density that a ray coming from a solid angle $d\omega'_j = \sin\theta'_j d\theta'_j d\phi'_j$ centered on direction (θ'_j, ϕ'_j) is reflected into another solid angle $d\omega'_{j+1} = \sin\theta'_{j+1} d\theta'_{j+1} d\phi'_{j+1}$ centered on direction $(\theta'_{j+1}, \phi'_{j+1})$. The same definition holds for the function τ. The type of interaction T is simulated by generating a random variable u uniformly distributed in $[0, 1]$, such that a reflection occurs (T^R) if $0 \le u \le \rho_p(\theta'_j, \phi'_j)$, a transmission occurs (T^T) if $\rho_p(\theta'_j, \phi'_j) < u \le \rho_p(\theta'_j, \phi'_j) + \tau_p(\theta'_j, \phi'_j)$, and an absorption occurs (T^A) if $\rho_p(\theta'_j, \phi'_j) + \tau_p(\theta'_j, \phi'_j) < u \le 1$. The scattering direction Ω'_{j+1} is simulated on the basis of the knowledge of the incoming direction Ω'_j, the surface normal to the intersection point Ω_L and the reflection or transmission scattering functions only. In the case of reflection, for instance, the scattering direction ${}^R\Omega'_{j+1}$ is computed with

$${}^R\Omega'_{j+1} = \Psi(\theta'_j, \phi'_j, u_1, u_2) \quad (4)$$

where $\Psi(\theta'_j, \phi'_j, u_1, u_2)$ is a random variate generated on the basis of the normalized function $\rho(\theta'_j, \phi'_j; \theta'_{j+1}, \phi'_{j+1})/\rho_p(\theta'_j, \phi'_j)$ and u_1, u_2 are uniformly distributed in [0, 1]. The expression for $\rho_p(\theta'_j, \phi'_j)$ can be found in [15] in the case of a Lambertian surface and in [16] in the case of a specular one.

2) Propagation in a Scattering Medium: Scattering media are characterized by a set of probability-distribution functions and a sampling process. Basically, these functions represent the effects of the structural properties of the medium (density and orientation of the scatterers) and of the optical properties of the scattering elements. These functions are applied to compute ray trajectories from their entrance into the medium to their eventual absorption or escape. A discrete random-walk process in this medium will therefore be completely specified by the simulation of the probability of collisions (interception points) and the scattering directions.

a) *Computation of the interaction point:* In a spatially homogeneous medium, distances between interactions are exponentially distributed, such that the probability of covering a path length d between two consecutive interactions in the direction Ω_j is given by

$$p(\Omega_j, d) = 1 - \exp[-\tau(\Omega_j) d] \quad (5)$$

where $\tau(\Omega_j)$ is the optical thickness of the medium in the direction Ω_j. The actual ray-path length covered in that medium after an interaction is calculated as

$$d_a(\Omega_j) = -\frac{1}{\tau(\Omega_j)} \ln u, \qquad u \in [0, 1] \quad (6)$$

such that an interaction with the medium will occur if $d_a(\Omega_j) < d_m(\Omega_j)$, where $d_m(\Omega_j)$ is the maximum distance that the ray can physically cover in the finite medium in direction Ω_j. The position P_{j+1} of the collision is calculated as

$$P_{j+1} = P'_j + \Omega_j d_a(\Omega_j) \quad (7)$$

with $\|\Omega_j\| \equiv 1$, and P'_j is the position where the ray first intersects the envelope of the medium. The appendix gives the formulation of $\tau(\Omega_j)$ in the case of finite-size-oriented scatterers.

b) *Computation of the scattering direction:* The scattering direction is determined as previously described [(1) and (2)] or with a phase function $\Gamma(\theta_j, \phi_j; \theta_{j+1}, \phi_{j+1})$ when the scatterer size is small enough, with respect to the wavelength. In this case, we simulate the scattering with an elementary volume. The ray will be absorbed if $\alpha(\theta_{j+1}, \phi_{j+1}) < u$ with $u \in [0, 1]$. $\alpha(\theta_j, \phi_j)$ is the so-called "single-scattering albedo" and

$$\alpha(\theta_j, \phi_j) = \int_{4\pi} \Gamma(\theta_j, \phi_j; \theta_{j+1}, \phi_{j+1}) \, d\omega_{j+1}. \quad (8)$$

D. Measurements

The computed ray paths $L_{k=1,\ldots,N}$ include the exact position of each collision point with the associated intercepted-object identification and type of interaction. It is, therefore, possible to extract very easily any kind of statistics from these trajectories, such as the mean free-path distribution or the vertical-extinction profile in the canopy. Furthermore, these measurements may be applied selectively to the ray trajectories by using virtual filters. Specific studies may indeed require knowledge of the separate contributions of the different components of the scene (e.g., leaves, branches, and soil) to differentiate the single and the multiple scattering or to extract statistics on the type of scattering. Virtual filters can be

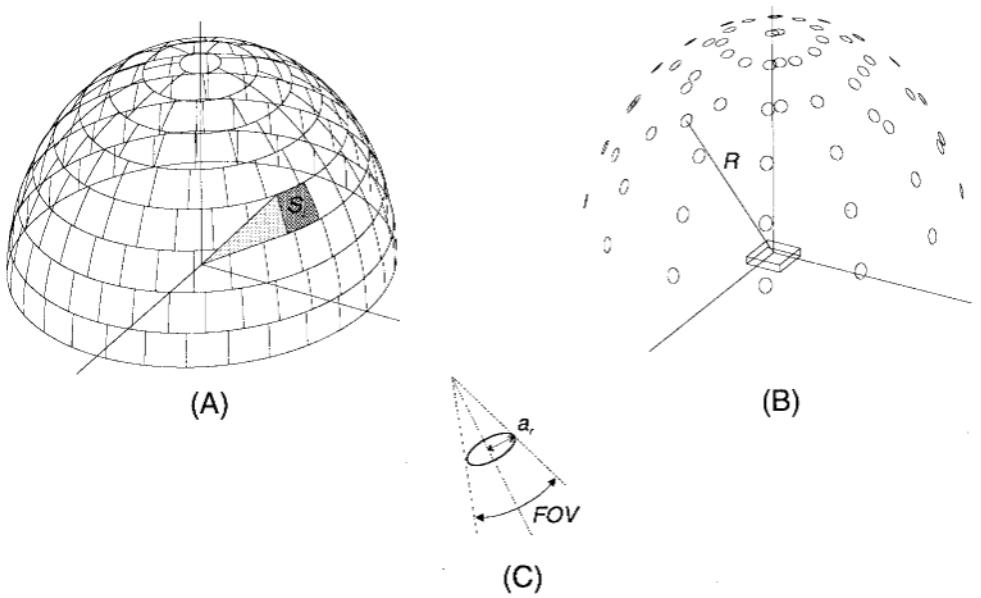

Fig. 2. Bidirectional reflectance factor measurements: (a) division of the hemisphere into equal area patches to estimate the BRF, as observed at very large distances, (b) simulation of goniometer observations of radius R with a detector of aperture $A_r = \pi a_r^2$, and (c) given field-of-view.

optionally associated with each measurement to select only ray trajectories that fulfill a set of conditions, such as the number of interactions, the collision with specific objects, or the way rays terminate (absorbed or scattered out of the scene). Since different measurements can be defined simultaneously, these filters allow extraction of different information from a single execution of the program and thereby save computer time.

To estimate the bidirectional reflectance factor (BRF), the hemisphere above the scene is divided into n_e patches of equal area $S_{i=(l,m)} = 2\pi/n_e$ [Fig. 2(a)]. The hemisphere is divided into k zones of area $Z_m$with $m \in [1, k]$, each of which is divided into $j(m) = Z_m/S_{i=(l,m)}$ elementary areas. The width $\Delta\theta_m (m = 1, \cdots, k)$ of a zone is adjusted in order that $j(m)$ is an integer number and the azimuthal length $\Delta\phi_l [l = 1, \cdots, j(m)]$ of an elementary area is approximately equal to $\Delta\theta_m$. The BRF $f_{i=(l,m)}$ in the direction of the solid angle defined by the elementary surface $S_{i=(l,m)}$ is calculated according to [17]

$$f_i(\theta_0, \phi_0;\ \Delta\theta_i, \Delta\phi_i) = \frac{\pi N_i}{N\Delta\Omega_i}, \qquad i = 1, \cdots, n_e \tag{9}$$

where N_i is the number of rays that cross S_i; N is the total number of generated rays; and $\Delta\Omega_i$ is the projected solid angle corresponding to the elementary surface S_i. If the hemisphere is located at infinity, only the direction of an escaped ray determines the outgoing solid angles S_i, whatever the origin of the ray. Equation (9) is, therefore, useful for direct comparisons with other BRF models. However, for comparisons with observations, it is desirable to reproduce as faithfully as possible the actual measurement conditions, such as the detector aperture A_r and field-of-view ψ. To allow this, the opportunity of simulating front-of-detector BRF g_i of a typical instrument located at a given distance R from the center of the target [Fig. 2(b)] has been added, where

$$g_i(\theta_0, \phi_0;\ \theta_i, \phi_i) = \frac{\pi N^{\psi}_{A_r,i} R^2}{N A_r \cos\theta_i}. \tag{10}$$

$N^{\psi}_{A_r,i}$ refers to the number of rays hitting the detector of area A_r located in (R, θ_i, ϕ_i) with a central direction included in the cone defined by the detector field-of-view [Fig. 2(c)]. Because the ray paths are computed without any probability-weighting mechanism, it turns out that statistical estimations of target radiative properties, as given by (9) and (10), are fairly simple and straightforward to derive. In the same way, any kind of statistics on the radiation regime can be very easily implemented.

III. Model Evaluation

The "verification" of a numerical model (the establishment of its truth) or the "validation" of a natural system (its legitimacy) is extremely difficult, if not impossible, to achieve [18]. The adequacy of a model to represent specific conditions can, however, be confirmed by comparisons with laboratory tests. These direct comparisons simply demonstrate that a model matches observations over a particular range of conditions under consideration. Although we individually evaluated all the functions implemented in the model in simple situations, it would not be practically possible to evaluate every combination of these functions since Raytran is not dedicated to a specific scene or problem. It is, however, desirable to assess the accuracy that can be reached for different specific situations. Furthermore, the observations against which Raytran can be compared require the precise knowledge of the position, size, and shape of each element of the scene as well as their optical properties, simultaneously with the values of the bidirectional reflectance of the scene and the lighting conditions. Since such data sets may be difficult and costly

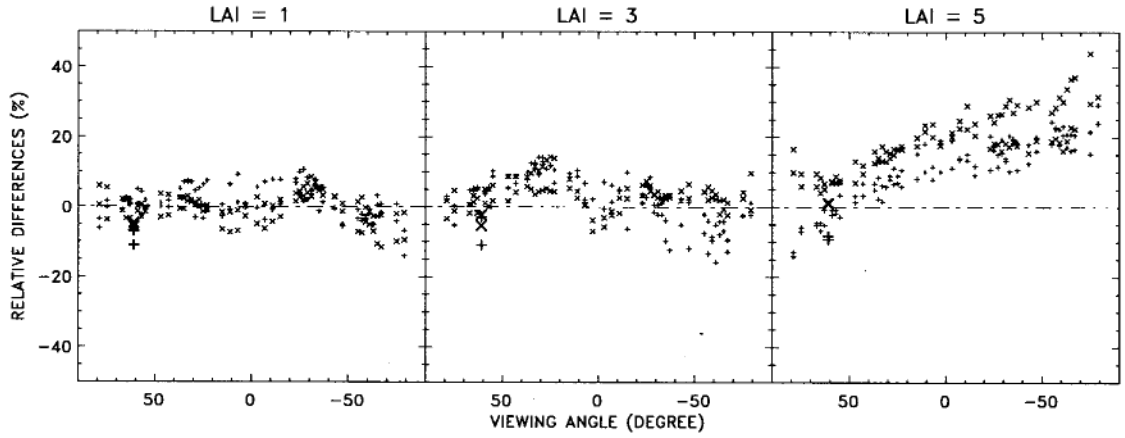

Fig. 3. Relative difference between the bidirectional reflectance factors in the red (indicated with a + symbol) and near-infrared (indicated with a × symbol) spectral regions computed with the Raytran and the Ross and Marshak models for the erectophile canopy, with LAI $= 1, 3,$ and 5 and an illumination zenith angle of 61°. Reflectance factors in the hot-spot directions are indicated with large symbols. Positive values indicate an overestimation of Raytran, with respect to RM.

to acquire for natural targets, comparisons have been done with other canopy reflectance models and observations of a man-made target whose characteristics are precisely known, avoiding additional assumptions on the representation of the target structural properties.

A. Comparison with Another Monte Carlo Code

First, we compared Raytran with another radiative transfer Monte Carlo model [4] (referred below as RM), which is very similar to Raytran in its principle. The RM model relies on the same assumptions concerning the physical description of light propagation. In addition, exactly the same scene architecture may be represented in both models. However, important conceptual differences between the two models remain. First, in the RM model, rays are traced by using a weighting mechanism adjusted after each collision, where the contribution to the bidirectional reflectance is estimated for every viewing angles. A ray path is stopped when its weight becomes too small. Second, the RM model permits the simulation of only one type of plant canopy architecture composed of circular leaves disposed along vertical cylindrical stems, while Raytran has almost no limitation on the represented scene complexity, illumination conditions, and ray-matter interaction models. Finally, the two models do not compute the BRF in exactly the same way. For a given viewing direction, Raytran accounts for all the rays in the solid angle defined by the patch corresponding to that direction [Fig. 2(a)], while RM accounts only for the rays in the unique direction of observation.

Comparisons have been carried out for canopies with leaf area index (LAI) of 1, 3, and 5, with illumination zenith angles of 31 and 61°, for a planophile- and an erectophile-leaf normal distribution. We considered two types of soil reflectance (Table I) in the red (RED) and near-infrared (NIR) spectral regions. We computed the mean relative difference R_d between two models estimated with

$$R_d = 100 \sum_{O_p} \frac{1}{N_p} \frac{\rho_{\text{Raytran}} - \rho_{\text{RM}}}{1/2(\rho_{\text{Raytran}} + \rho_{\text{RM}})} \qquad (11)$$

where ρ_{Raytran} and ρ_{RM} are the bidirectional reflectance factors of the Raytran and RM model, respectively, and N_p is the number of observations. For LAI $= 1$, R_d does not exceed 1%. The relative difference slightly increases as the LAI increases. When LAI $= 3$, $R_d = 5\%$, and for the dense canopy case (LAI $= 5$), the differences between Raytran and RM amounts to 15%. Fig. 3 shows the relative difference between the two models in the principal plane for the erectophile-leaf angular distribution and an illumination zenith angle of 61°. The systematic bias that can be observed when the LAI increases probably results from the fictitious fly technique that is applied in the RM model to compute the contribution to the BRF of each interaction point. Indeed, an interaction point contributes to the BRF only if there is no intercepting element between this point and the top of the canopy in the direction of observation, neglecting, therefore, a possible transmission through the leaves. In other words, leaves are assumed black when applying this variance-reduction technique. An increase in LAI raises the probability that a fictitious fly intercepts canopy elements and, therefore, also the apparent absorption, especially when the transmission is high, as it is the case in the near-infrared spectral region that can be seen in Fig. 3. The underestimation of the reflectances computed with the RM model has been reported elsewhere [19], except in the hot-spot direction. Indeed, in that specific direction, indicated with large symbols in Fig. 3, the points of the first interaction can always be seen by the observer and the fictitious fly is never intercepted. As a result, the difference between Raytran and the RM model is smaller in that particular direction, even when LAI $= 5$. In fact, in the hot-spot direction, Raytran slightly underestimates the reflectance factor because it always computes an average factor for a finite solid angle.

This comparison shows that is was worthwhile to design Raytran with a Monte Carlo scheme as close as possible to the actual radiative processes to avoid any bias resulting from the implementation of optimization techniques. However, to confirm this preliminary evaluation, it is necessary to compare our model with another canopy reflectance model based on a different numerical approach.

TABLE I
SPECTRAL VALUES FOR THE VARIOUS ELEMENTS OF THE SCENE (ρ = REFLECTANCE; τ = TRANSMITTANCE)

		RED		NIR	
Data set	Element	ρ	τ	ρ	τ
DRK	Leaves	0.075	0.050	0.500	0.450
	Stem	0.060	0.	0.350	0.
	Soil	0.100	0.	0.150	0.
BRT	Leaves	0.075	0.050	0.500	0.450
	Stem	0.060	0.	0.350	0.
	Soil	0.250	0.	0.350	0.

B. Comparison with a Homogeneous 3-D Model

Among the various numerical methods that have been developed to solve the equations of radiation transfer, the discrete-ordinate techniques provide a well-established approach in the case of homogeneous scattering media. Therefore, we have compared Raytran with a discrete-ordinate canopy reflectance model called IAPI2A [20]. This model evaluates the bidirectional reflectance through the numerical solution of the 3-D canopy radiative-transfer equation. To simplify the radiation-transfer formulation, the hot-spot effect is estimated only from the contribution of the single scattering of direct radiation and uncollided radiation reflected by the soil. The incoming and outgoing ray directions are assumed to be uncorrelated in the treatment of second- and higher order collisions. The structural properties of the medium are characterized by the scatterer area index λ, two parameters for the scatterer normal distribution (μ, ν), and the mean sun-fleck radius between the scatterers r. For the purpose of the comparison, it is necessary to represent an equivalent canopy with geometrical primitives, as required by the Raytran model. In the Raytran canopy, we assume that each scatterer can be represented by a disc of given radius r_s and normal orientation Ω_L. The canopy was represented as a parallelepipedic box of given height h and surface s filled with n_s discs quasirandomly located to keep the scatterers from intersecting. The angular distribution of the disc normals follows a β distribution $g_L(\mu, \nu)$ in the zenith direction and a uniform one in the azimuthal direction. This discrete canopy can be, therefore, very easily generated, provided the parameters h, s, n_s, and r_s and the function $g_L(\mu, \nu)$ are known. The scatterer area index λ is simply related to these parameters by

$$\lambda = \frac{\pi r_s^2 n_s}{s}. \tag{12}$$

It is desirable to derive an expression of λ that does not depend on the absolute size of the Raytran scene. Statistically, each scatterer is expected to occupy a mean elementary box whose volume is

$$V_s = \frac{sh}{n_s} = d_h^2 d_v \tag{13}$$

where d_h is the horizontal side of the parallelepiped and d_v the vertical one. A new parameter h_v is introduced to describe the ratio between the mean vertical and horizontal distance between the leaves, such that $d_v = d_h/h_v$ and

$$d_h = (h_v sh/n_s)^{1/3}. \tag{14}$$

This parameter controls the vertical density of the scatterers. We then normalize all the distances in the model by the d_h. Therefore, $r_{\hat{d}} = r_s/d_h$, and (14) may be rewritten as

$$d_{\hat{h}} = (h_{\hat{v}} h_{\hat{d}}/n_{\hat{s}}) = 1 \tag{15}$$

where $h_{\hat{v}} = h_v/d_h$ and the height of the canopy is equal to $h_{\hat{d}} = h_d/d_h$. $n_{\hat{s}} = h_{\hat{v}} h_{\hat{d}}$ is now the mean number of scatterers along the vertical direction. The main advantage of this normalized equation is that the expression of the scatterer-area density does not depend anymore on the actual size of the boxes or the total number of elements; it is simply equal to $\lambda = \pi r_{\hat{d}}^2 n_{\hat{s}}$. Clearly, small values of $r_{\hat{d}}$ represent a discrete canopy more similar to the ideal case of the turbid medium than larger ones, for which the intershadowing effects are stronger. The approximate relation for the mean sun fleck radius r is [21]

$$r(\theta_0) = r_0 \sqrt{\frac{\cos\theta_0}{G(\theta_0)\pi r_{\hat{d}}^2 h_{\hat{v}} y_t}} \tag{16}$$

where θ_0 is the direction of illumination; $G(\theta_0)$ is the Ross function (as given in the Appendix); and r_0 is the mean radius of the hole between the leaves at the top of the canopy, which is approximated by $r_0 = d_{\hat{h}}^2 - G(\theta_0)\pi r_{\hat{d}}^2$. The depth y_t of direct solar penetration in the canopy has been chosen equal to $h_{\hat{d}}$. As can be seen in (16), the mean sun-fleck radius is a function of the illumination zenith angle.

We computed the corresponding reflectances by using the optical data set BRT described in Table I for the soil and the leaves with an illumination zenith angle of 30°. The Raytran canopy is generated with 40 000 circular scatterers that are lit with 200×10^6 rays, providing a mean-estimated error lower than 1%, with a 95% confidence interval. All surfaces, including the soil, are assumed Lambertian. Fig. 4 shows the reflectance factors of uniform canopies in the NIR for LAI $= 1, 3$, and 8 and $r_{\hat{d}} = 0.17, 0.3$, and 0.5. These results show the very good agreement between Raytran and the discrete ordinates model. The relative difference between the two models is very small, around ±2% especially for small values of $r_{\hat{d}}$, i.e., when the structural properties of the medium come close to the turbid medium case. It can also be seen that Raytran underestimates the reflectance factor value around the hot spot, with respect to the IAPI2A model. The reason is similar to the one given in the previous section. This comparison also shows that both models account accurately for the multiple scattering. Indeed, the mean number of interactions ranges between 1.8 when LAI $= 1$ and 6.4 when LAI $= 8$.

C. Comparisons with Laboratory Measurements

It is desirable to evaluate the accuracy of Raytran against BRF measurements. These observations have been carried out by the Advanced Techniques Unit of the Space Applications Institute in the new goniometer facility. The European Goniometer (EGO) laboratory is a double T-angle iron structure composed of a platform that will receive the sample target and two rotating arcs, a quarter circle for the light source and a semicircle for a detector [22]. The system allows the

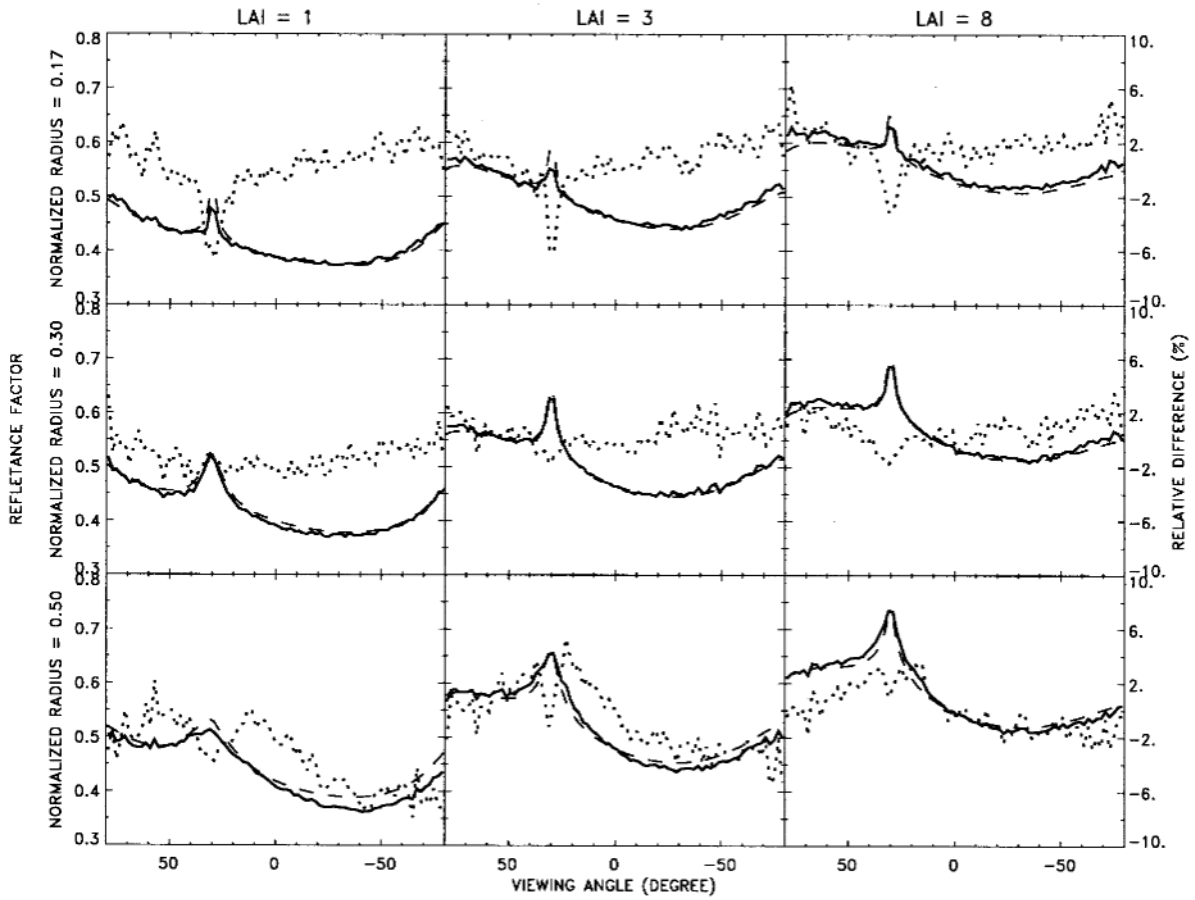

Fig. 4. Near-infrared reflectance factors in the principal plane for the Raytran model (solid line) and the IAPI2A model (dashed line) for a uniform-leaf normal distribution (scale on the left). The illumination zenith angle is 30°. The dotted lines show the relative difference between the two models (scale on the right). Positive values indicate an overestimation of Raytran, with respect to IAPI2A.

independent positioning of the light source and the detector anywhere on a 2-m radius hemisphere around the target and, thereby, the measurement of biconical reflectances.

The specifications of the artificial target must be carefully thought out if it is to be used to evaluate the model. As previously explained, the structural properties of a natural scene would be difficult to characterize. Therefore, for the purposes of this evaluation, we worked on simple man-made surfaces, whose geometrical and optical properties can be characterized *a priori* in the laboratory and represented explicitly for Raytran simulations. Specifically, the choice of the target has been motivated by the following requirements: 1) the target should be easy to manufacture; 2) the geometry of the rough surface should be relatively easy to characterize and simple to represent in Raytran; 3) the bidirectional reflectance anisotropy of the target must be clearly observed; and finally, 4) the optical properties of the material should be known or independently measurable. The target has accordingly been designed as a 25 × 25-cm matrix or lattice of cubes over a plane surface [Fig. 5(a)] made of duralumin A-U4GUNI3579. To ensure uniformity of properties, the rows of cubes have actually been carved out of a thick plate [Fig. 5(b)]. All vertical and horizontal exposed faces have been sanded to get an average surface microroughness σ_r of 1.65 μm. The shape factor, i.e., the ratio between the sides s_c of the cubes and the distance d_c between the cubes, has been chosen to enhance the target structural effects and are such that $s_c = (5/3)\,d_c$, with $d_c \approx 2$ mm and $s_c \approx 3.3$ mm. The tolerance of the cut is ±0.1 mm.

The lighting source is a compact, self-contained He–Ne laser emitting at 0.6328 μm. A beam expander provides a beam with a usable diameter of 48 mm. The detector is a simple silicon photo-diode with an active area of 100 mm^2. To control the field-of-view of the detector, a 100-mm long tube with a diameter of 50 mm is placed in front of it, ensuring a field-of-view of 28°. Illumination zenith angles are 3, 26, and 56° and every 15°, with respect to the rows in azimuth. Observations have been performed every 10° in zenith and 15° in azimuth. A Spectralon panel lit with an illumination zenith angle of 3° was used for the calibration of the data to evaluate the reflectance factor.

Modeling the bidirectional reflectance of the lattice target first requires the characterization of the bidirectional properties of the cube sides. For that purpose, we prepared a third target consisting simply of a flat panel of duralumin with the same finishing process. The Torrance and Sparrow model [23] has been used to characterize the BRF of this plate. This model has been specifically designed to simulate the reflectance of rough surfaces composed of randomly distributed mirror-like microfacets. With the notations used earlier, the scattering-

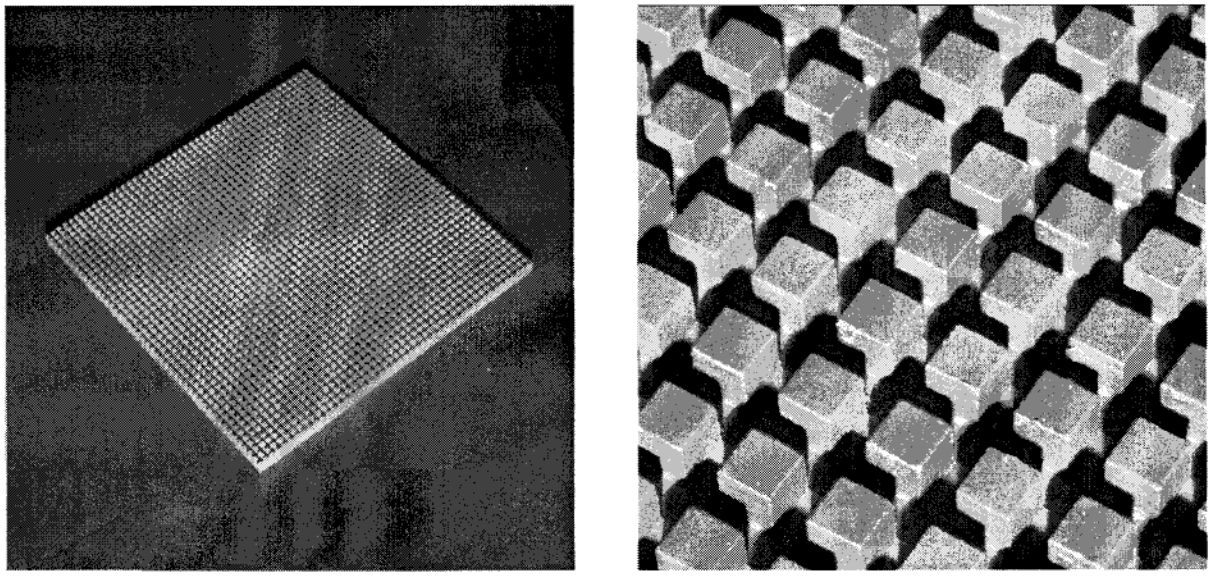

(a) (b)

Fig. 5. Custom-designed 25 × 25-cm target made of a lattice of cubes for comparison with goniometer measurements: (a) general view of the target and (b) detail of the lattice of cubes.

reflection function is expressed in (17), shown at the bottom of the page, where D and S are scaling factors for the diffuse and specular contributions, respectively.

- $F(\theta'_p, \hat{n}_{12})$ is the Fresnel reflection, in which $\cos\theta'_p = (\Omega'_j \cdot \Omega'_H)$, with $\Omega'_H = (\Omega'_j + \Omega'_{j+1})/2$. Since the duralumin is a conducting material, the index of refraction $\hat{n}_{12}$ is complex and is equal to $\hat{n}_{12} = n(1 + ik)$, where k is the extinction coefficient.
- $T(\Omega'_j, \Omega'_{j+1})$ is the microfacet distribution. This distribution function indicates the number of microfacets oriented in the direction Ω'_{j+1} and is given by the Beckmann distribution [24]

$$T(\Omega'_j, \Omega'_{j+1}) = \frac{\exp(-\tan^2\beta/\sigma_m^2)}{4\sigma_m^2 \cos^4\beta} \tag{18}$$

  where $\sigma_m \in [0, 1]$ is the rms slope of the facets and $\beta = \arccos(\Omega'_L \cdot \Omega'_H)$. Small values of m (<0.2) characterize a smooth surface, while larger ones simulate rough surfaces that spread the specular peak.
- $A(\Omega'_j, \Omega'_{j+1})$ is a geometric attenuation term accounting for the amount by which facets shadow and mask each other [25].

The parameters of (17) have been retrieved by inverting the Torrance–Sparrow model against the reflectance factor of the lattice target by using a method based on the genetic algorithms [26]. The following values have been retrieved: $D = 0.2261$, $S = 2.3917$, $n = 1.2311$, $k = 1.1838$, and $\sigma_m = 0.372$. The value of a least-square fit between observations and simulations is equal to 1.397 for a rms error of 0.0313. The corresponding density function is numerically integrated with the 32-point Gaussian-quadrature method and stored in a lookup table. The associated random variate Ψ is computed with a rejection scheme [27].

The structural properties of the lattice target are simulated with boxes laid out on a square polygon base within Raytran. The laser beam is simulated with a circular energy source whose normal is oriented through the center of the target. The emitted rays are parallel to that normal. The scene is lit with 200 × 10^6 rays, which insures an estimated error of the simulated reflectance better than 0.5%. The reflectance factor is computed with (10), which accounts for the aperture and field-of-view of the detector. The mean number of interaction per ray is 1.2. Consequently, the contribution resulting from the multiple scattering may not be neglected.

Fig. 6 compares the modeled reflectance factors to the observed ones for an illumination azimuth angle of 45°, with respect to the rows. Simulations reproduce correctly the reflectance variations, both in shape and intensity, due to the row structure of the cubes, although some quantitative differences are noticeable. Two major sources of discrepancy should be explored further: the inaccuracies of the representation of the target optical and structural properties and the errors of measurement.

As already mentioned, the Torrance and Sparrow model does not fit exactly the observed reflectances of the reference panel. The rms error between the observations and the simulations is equal to 0.0284, which is very close to the rms obtained for the reference duralumin panel. Moreover, observations for an illumination zenith angle of 56° show backscattering effects that may be due to the hot-spot effect

$$\rho(\theta'_j, \phi'_j; \theta'_{j+1}, \phi'_{j+1}) = \frac{1}{\pi}\left[D\cos\theta'_{j+1} + S\frac{F(\theta'_p, \hat{n}_{12})T(\Omega'_j, \Omega'_{j+1})A(\Omega'_j, \Omega'_{j+1})}{4\cos\theta'_j\cos\theta'_{j+1}}\right]d\omega'_{j+1} \tag{17}$$

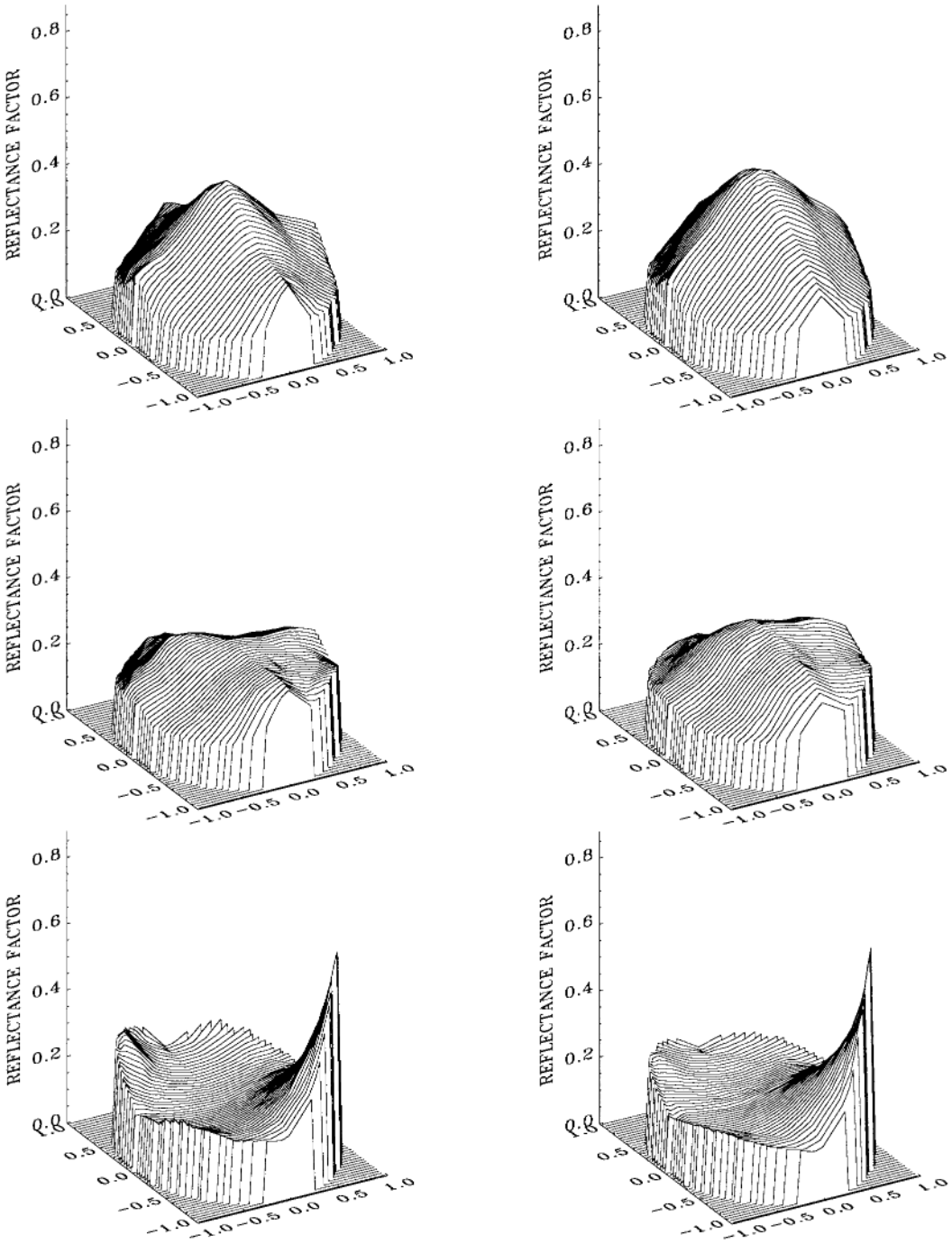

Fig. 6. Observations (left column) of the reflectance factors of the lattice target and simulations (right column) for three different illumination zenith angles: 3 (first row), 26 (second row), and 56° (third row). The values are plotted in cylindrical coordinates. The distances from the origin of the horizontal axes represent the cosine of the zenith angle of observation. The lattice of cubes is illuminated with an azimuth angle of 45°, with respect to the rows.

or coherent backscattering [28] that are not represented in the Torrance–Sparrow model. In addition, the regularity of the target macrostructure (there are only five different normal directions) makes the target reflectance anisotropy particularly sensitive to the material directional properties. In natural media, the angular dispersion of the scattering elements is much wider, so that the effects of their directional properties are averaged. Consequently, further efforts are needed to improve the characterization of the surface optical properties.

Among the other possible sources of differences, the problem of measurement inaccuracies must be pointed out. First, the Spectralon reference panel is not a perfect Lambertian surface [29], even for an illumination zenith angle of 3°; the reflectance at a zenith angle of observation of 56° is 12% lower than at the nadir. As a result, normalized measured reflectances should be overestimated at large zenith angles of observations and underestimated at lower ones. Second, the comparison of the left and right side of the reflectance factors,

with respect to the principal plane in the case of a row-aligned azimuthal illumination, has revealed a bias in the observations, with a maximum relative difference of 40% in the specular direction for an illumination at 56°. Further investigations are required to determine if this bias may be due to a defect of the goniometer structure. To the extent that such a defect can be identified and quantified, it will be possible to simulate it with Raytran and therefore to correct the data for this instrumental effect. Comparisons with laboratory measurements thus show the capability of Raytran to reproduce actual observed reflectance factors of a fully documented target, even in the case of non-Lambertian surfaces.

IV. Discussion and Perspectives

In this paper, we emphasized the strength of Monte Carlo ray-tracing techniques to describe the transfer of radiation in scenes of arbitrary complexity. Indeed, these techniques allow the description of a variety of 3-D scenes with realistic optical properties under simulated natural or artificial illumination conditions. Raytran allows the study of a number of radiative transfer issues in relation to the remote-sensing observation of terrestrial surfaces, such as sensitivity studies, target spectral signature analysis, sensor and retrieval procedure evaluation, etc. Since ray paths are generated in a straightforward, physically meaningful way, the numerical scheme is not affected by systematic bias, and the extraction of any kind of information concerning the radiation regime in the target is easy. Indeed, the optimization of the Monte Carlo procedure does not rely on any variance-reduction technique, but on an efficient parallelization of the code. Furthermore, the filters that can be associated with each measurement allow very specific problems to be addressed. These advantages, in conjunction with the possibility of assigning elaborate ray-matter interaction models, whatever the type, size, and structural complexity of the target, and the fact that multiple scattering is exactly represented, are definitively original features.

We have also shown that Raytran compares favorably with well-established canopy reflectance models. However, the description of the scatterer optical properties to achieve good quantitative accuracies remains a major issue, as has been demonstrated by comparison with laboratory measurements. While bidirectional reflectance models have already been developed for bare soils, little work has been dedicated so far to the description of the bidirectional reflectance of a single plant leaf as a function of its morphological and physiological properties. Raytran has been applied to this problem, as reported elsewhere [12].

Generally speaking, the accuracy with which the scenes can be characterized determines the relevance of the results. Additional investigation would be necessary to evaluate the level of detail that needs to be achieved to represent realistic heterogeneous plant canopies. These efforts will require field measurements with a detailed description of the architectural properties of the scene and the optical characteristics of its elements. Alternatively, models can be used to describe plant architecture by using appropriate techniques, such as L-systems, as suggested in previous studies [30], [31].

Within the framework of canopy-reflectance-modeling activities, a large number of issues can be addressed with Raytran. This model can improve the interpretation of the hot-spot parameterization through an explicit description of the position of each scattering element. This capability will permit further improvement of the radiative-transfer formulation in media composed of finite-size and oriented scatterers [32]. The validation of algorithms developed to extract quantitative information from spaceborne observations represents another challenging issue. In this respect, the capability of representing highly realistic scenes should permit to produce well-documented synthetic reflectance data sets. In turn, these data sets can be used to evaluate spectral indexes or the inversion of simple canopy reflectance models [33]. Future developments of Monte Carlo ray-tracing models will concern the better representation of the actual observation conditions to allow the simulation of future sensors. As a first step in that direction, we have already simulated a laser altimeter sensor [34], which records the complete history of the reflected pulses [35].

Appendix
Optical Thickness of Pseudoturbid Media

Uniform canopies may be represented as homogeneous scattering media provided that the finite size and orientation of the leaves are taken into account. The structural properties of such media can be described as a function of the leaf area density (Λ), the scatterer normal distribution, and finally, the mean horizontal (a_h) and vertical (a_v) areas between the scatterers, as defined in [35]. The simulation of a collision in that medium is expressed as a function of its optical thickness $\tau(\Omega_j)$ in direction Ω_j of the incoming radiation is simply defined as [36]

$$\tau(\Omega_j) = \Lambda\sigma(\Omega_j) \tag{19}$$

and has the dimension of the inverse of distance. $\sigma(\Omega_j)$ is the total interaction cross section and is defined by the Ross function [37]

$$\sigma(\Omega_j) = G(\Omega_j) = \frac{1}{2\pi}\int_{2\pi} g_L(\Omega_L)|\Omega_j \cdot \Omega_L| d\Omega_L. \tag{20}$$

The function $g_L(\Omega_L)/2\pi$ is the leaf normal-distribution function. To save computer time, the $G(\Omega_j)$ function is numerically integrated once and for all and stored in a lookup table. After the first scattering, (20) must be slightly modified to take into account the correlation between the incoming and the outgoing directions. In this case, the ray being scattered back exactly in the incoming direction must obviously be able to exit the medium without further interaction. To express this "hot-spot" phenomenon, a geometrical-statistical approach has been adopted [21]. We present here only the adaptation of the method in the case of a nonplane parallel medium. Let Ω_L be the normal to the surface of the object, which describes the medium at the intersection point P_j' with the incoming ray (Fig. 7). We will assume that the horizontal a_h and vertical a_v areas between the scatterers are circular and that the size of the medium's spatial extension is much larger than a_h and

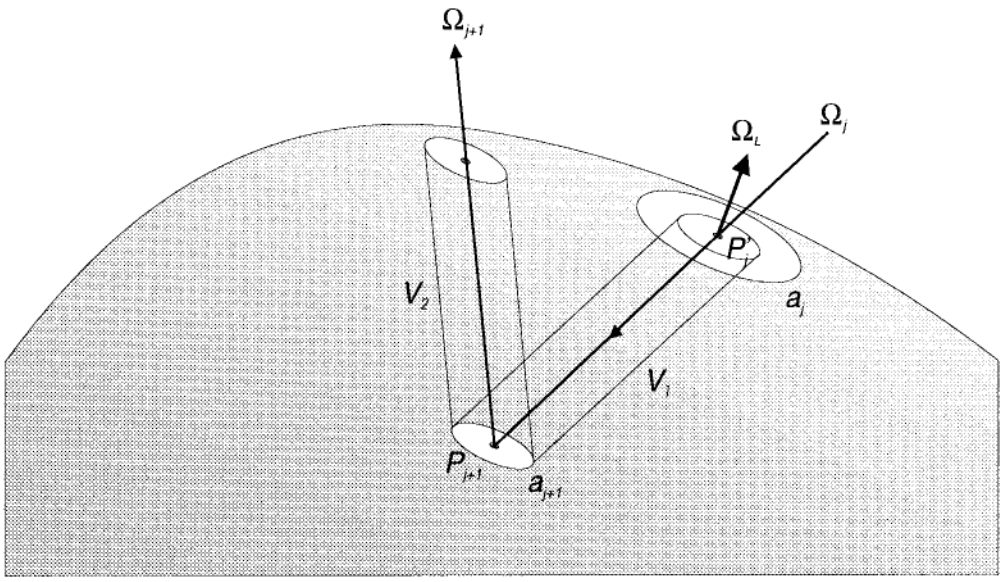

Fig. 7. Geometry of illumination of a homogeneous scattering medium. P'_j is the point where the ray of direction Ω_j intersects with the medium envelope. Ω_L is normal to the surface in P'_j. a_j defines the surface of the corresponding beam projected in a plane perpendicular to Ω_L. P_{j+1} is the simulated point of interaction in the medium, and a_{j+1} is the section of the beam at that point. V_1 and V_2 are the cylinders that define the incoming and outgoing beams.

a_v, such that the surface may be assumed locally plane in P'_j. The projection a_j of a_h and a_v in P'_j on a plane perpendicular to $\Omega_L(\theta_L, \phi_L)$ is equal to

$$a_j = a_h \cos\theta_L + a_v \sin\theta_L. \tag{21}$$

Instead of tracing a single ray, the trajectory of a beam in the medium will be considered. Hence, a_j represents the section of this beam in P'_j. This section decreases exponentially until P_{j+1} along the direction Ω_j, as follows:

$$a_{j+1} = a_j \exp[-\tau(\Omega_j) d_a(\Omega_j)] \tag{22}$$

where $d_a(\Omega_j)$ is the distance between P'_j and P_{j+1} which is the point of interaction in the medium as given by (7). The area a_{j+1} characterizes the section of the beam, projected on a plane perpendicular to Ω_L, along the trajectory $P'_j \rightarrow P_{j+1}$. This area and the direction Ω_{j+1} define, therefore, a cylinder V_2 that shares a common basis in P_{j+1} with the cylinder V_1 in the direction Ω_j. Consequently, as long as the rays scattered in P_{j+1} remain in the volume common to the two cylinders, the optical thickness is zero. The effective interaction cross section in the direction Ω_{j+1} should be proportional to the ratio V/V_2, where V is the proportion of V_2 not common to V_1

$$\sigma(\Omega_{j+1}) = \frac{V}{V_2} G(\Omega_{j+1}). \tag{23}$$

The expression of V/V_2 is given by Verstraete [21], which differs in that, in the present case, the plane parallel system, which is used to derive the expression, is perpendicular to the direction Ω_L. After the second collision and for higher order scattering, the relation (20) is used to compute the optical thickness. The normal Ω_L at the simulated collision points P_{j+1} is generated with the following distribution [15]:

$$p(\Omega_L) = \frac{g_L(\Omega_L)|\Omega_j \cdot \Omega_L|}{2\pi G(\Omega_j)}. \tag{24}$$

The direction Ω_L is sampled with a rejection method.

ACKNOWLEDGMENT

This research would not have been possible without the generous access to the Centro Svizzero di Calcolo Scientifico (CSCS) in Manno, Switzerland. The authors are grateful to Dr. A. Sieber and the EGO staff for acquiring and providing the bidirectional reflectance data on the duralumin and Spectralon panels and to J. Iaquinta and A. Marshak for providing their computer codes. They thank B. Pinty for fruitful discussions and extensive comments on this paper.

REFERENCES

[1] D. S. Kimes and J. A. Kirchner, "Radiative transfer model for heterogeneous 3-D scenes," *Appl. Opt.,* vol. 21, pp. 4119–4129, 1982.
[2] S. Chandrasekhar, "On the radiative equilibrium of a stellar atmosphere. II," *Astrophys. J.,* vol. 100, pp. 76–86, 1944.
[3] R. B. Myneni, G. Asrar, and F. G. Hall, "A three-dimensional radiative transfer method for optical remote sensing of vegetated land surfaces," *Remote Sens. Environ.,* vol. 41, pp. 105–121, 1992.
[4] J. K. Ross and A. L. Marshak, "Calculation of canopy bidirectional reflectance using the Monte Carlo method," *Remote Sens. Environ.* vol. 24, pp. 213–225, 1988.
[5] N. S. Goel, I. Rozehnal, and R. L. Thompson, "A computer graphics based model for scattering from objects of arbitrary shapes in the optical region," *Remote Sens. Environ.,* vol. 36, pp. 73–104, 1991.
[6] C. C. Borel, S. A. W. Gerstl, and B. J. Powers, "The radiosity method in optical remote sensing of structured 3-D surfaces," *Remote Sens. Environ.,* vol. 36, pp. 13–44, 1991.
[7] B. Pinty and M. M. Verstraete, "On the design and validation of bidirectional reflectance and albedo models," *Remote Sens. Environ.* vol. 41, pp. 155–167, 1992.
[8] M. M. Verstraete and Y. M. Govaerts, "Modeling the scattering of light in arbitrarily complex media: Motivation for a ray tracing approach," Inst. Remote Sensing Applicat., CEC Joint Res. Centre, Ispra, Italy, Tech. Rep. EUR 15790 EN, 1994.
[9] J. M. Hammersley and D. C. Handscomb, *Monte Carlo Methods.* London, U.K.: Methuen, 1964.
[10] P. Shirley, C. Y. Wang, and K. Zimmerman, "Monte Carlo techniques for direct lighting calculations," *ACM Trans. Graph.,* vol. 15, pp. 1–36, 1996.
[11] Y. M. Govaerts and M. M. Verstraete, "Development and parallelization of a Monte Carlo ray tracing code for radiative transfer modeling: Initial lessons from using the Cenju-3 machine," *Speedup J.,* vol. 10, pp. 62–67, 1996.

[12] Y. M. Govaerts, S. Jacquemoud, M. M. Verstraete, and S. L. Ustin, "Three-dimensional radiation transfer modeling in a dicotyledon leaf," *Appl. Opt.,* vol. 35, pp. 6585–6598, 1996.
[13] M. E. Mortenson, *Geometric Modeling.* New York: Wiley, 1985.
[14] J. Arvo and D. Kirk, "A survey of ray tracing acceleration techniques," in *An Introduction to Ray Tracing,* A. S. Glassner, Ed. London, U.K.: Academic, 1989, pp. 201–262.
[15] V. S. Antyufeev and A. L. Marshak, "Monte Carlo method and transport equation in plant canopies," *Remote Sens. Environ.,* vol. 31, pp. 183–191, 1990.
[16] A. S. Glassner, "Surface physics for ray tracing," in *An Introduction to Ray Tracing,* A. S. Glassner, Ed. London, U.K.: Academic, 1989, pp. 121–160.
[17] J. K. Ross and A. L. Marshak, "The influence of leaf orientation and the specular component of leaf reflectance on the canopy bidirectional reflectance," *Remote Sens. Environ.* vol. 27, pp. 251–260, 1989.
[18] N. Oreskes, K. Shrader-Frechette, and K. Belitz, "Verification, validation, and confirmation of numerical models in Earth sciences," *Science,* vol. 263, pp. 641–646, 1994.
[19] S. Liang and A. H. Strahler, "An analytical BRDF model of canopy radiative transfer and its inversion," *IEEE Trans. Geosci. Remote Sensing,* vol. 31, pp. 1081–1092, Sept. 1993.
[20] J. Iaquinta, "Champs de rayonnement emergeant des surfaces terrestres: Modélisation et inversion dans le cas de milieux optiquement finis et couplés avec une couche atmosphérique," Ph.D. dissertation, Blaise Pascal Univ., 1995.
[21] M. M. Verstraete, B. Pinty, and R. E. Dickinson, "A physical model of the bidirectional reflectance of vegetation canopies; Part 1: Theory," *J. Geophys. Res.,* vol. 95, pp. 11 775–11 765, 1990.
[22] C. Koechler, B. Hosgood, G. Andreoli, G. Schmuck, J. Verdebout, A. Pegoraro, J. Hill, W. Mehl, D. Roberts, and M. Smith, "The European optical goniometric facility: Technical description and first experiments on spectral unmixing," in *IGARSS'94,* Pasadena, CA, pp. 2375–2377.
[23] K. E. Torrance and E. M. Sparrow, "Theory for off-specular reflection from roughened surfaces," *J. Opt. Soc. Amer.,* vol. 57, pp. 1105–1114, 1967.
[24] R. L. Cook and K. E. Torrance, "A reflectance model for computer graphics," *Comput. Graph.,* vol. 15, pp. 307–316, 1981.
[25] J. F. Blinn, "Models of light reflection for computer synthesized pictures," *Comput. Graph.,* vol. 11, pp. 192–198, 1977.
[26] J. M. Renders and S. P. Flasse, "Hybrid methods using genetic algorithms for global optimization," *IEEE Trans. Syst., Man, Cybern.,* vol. 26, pp. 243–258, 1996.
[27] L. Devroye, *Non-Uniform Random Variate Generation.* New York: Springer-Verlag, 1986.
[28] B. H. Hapke, R. M. Nelson, and W. D. Smythe, "The opposition effect of the moon: The contribution of coherent backscatter," *Science,* vol. 260, pp. 509–511, 1993.
[29] S. P. Flasse, M. M. Verstraete, B. Pinty, and C. J. Bruegge, "Recent advances in sensors, radiometric calibration, and processing of remotely sensed data," in *Proc. SPIE 1938*, Orlando, FL, 1993, pp. 100–108.
[30] N. S. Goel, L. B. Knox, and J. M. Norman, "From artificial life to real life: Computer simulation of plant growth," *Int. J. General Syst.,* vol. 18, pp. 291–319, 1991.
[31] Y. M. Govaerts and M. M. Verstraete, "Applications of the L-systems to canopy reflectance modeling in a Monte Carlo ray tracing technique," in *Fractals in Geoscience and Remote Sensing,* G. G. Wilkinson, L. Kanellopoulos, and J. Mégier, Eds. Joint Res. Centre European Commission, Ispra, Italy, 1994, pp. 211–236.
[32] N. Gobron, B. Pinty, M. M. Verstraete, and Y. M. Govaerts, "A semi-discrete model for the scattering of light by vegetation," *J. Geophys. Res.,* vol. 102, pp. 9431–9446, Apr. 1997.
[33] Y. M. Govaerts and M. M. Verstraete, "Evaluation of the capability of BRDF models to retrieve structural information on the observed target as described by a tridimensional ray tracing code," in *European Symp. Satellite Remote Sensing, Proc. SPIE 2314.* E. Mougin, K. J. Ranson, and J. A. Smith, Eds. Rome, Italy, 1995, pp. 9–20.
[34] D. J. Harding, J. B. Blair, E. Rodriguez, and T. Michel, "Airborne laser altimetry and interferometric SAR measurements of canopy structure and sub-canopy topography in the Pacific Northwest," in *2nd Topical Symp. Combined Opt.-Microwave Earth Atmos. Sensing (COMEAS'95),* Atlanta, GA, pp. 22–24.
[35] Y. M. Govaerts, "A model of light scattering in three-dimensional plant canopies: A Monte Carlo ray tracing approach," Space Applicat. Inst., JRC, Tech. Rep. EUR 16394 EN, 1996.
[36] M. M. Verstraete, "Radiation transfer in plant canopies: Transmission of direct solar radiation and the role of leaf orientation," *J. Geophys. Res.,* vol. 92, pp. 10 985–10 995, 1987.
[37] J. Ross, *The Radiation Regime and Architecture of Plant Stands.* Boston, MA: Junk, 1981.

Yves M. Govaerts received the Ph.D. degree in physics from the Université Catholique de Louvain, Louvain-la-Neuve, Belgium, in 1995.

He was with the Royal Meteorological Institute of Belgium as a Research Scientist from 1990 to 1993. From 1993 to 1997, he was with the Space Applications Institute, Ispra, Italy. Since 1997, he has worked for Eumetsat, Darmstadt, Germany. His principal research fields are radiative transfer modeling and the development of retrieval algorithms for remote sensing applications. He has worked on the design of vegetation indexes for the MERIS instrument on the ESA Envisat platform.

Michel M. Verstraete (M'95) received the License en physique from the Université Catholique de Louvain, Louvain-la-Neuve, Belgium, in 1974, the License Spéciale en géophysique from the Université Libre de Bruxelles, Bruxelles, Belgium, in 1976, and both the M.Sc. degree in meteorology and the D.Sc. degree in atmospheric sciences from the Massachusetts Institute of Technology, Cambridge, in 1978 and 1985, respectively.

He was with the World Meteorological Organization (WMO) in Geneva, Switzerland, and Nairobi, Kenya, from 1979 to 1981. He was then with the National Center for Atmospheric Research (NCAR), Boulder, CO, from 1982 to 1989. He taught at The University of Michigan, Ann Arbor, from 1989 to 1990. He is currently with the Space Applications Institute (SAI), Ispra, Italy. He is Co-Investigator of the MISR Science Team of NASA/JPL. His initial work on topics such as the modeling of atmosphere-biosphere interactions and desertification lead him to his current interest in the quantitative exploitation of satellite remote-sensing data for the detection and characterization of terrestrial surface properties.

Dr. Verstraete is a member of various scientific advisory committees of the European Space Agency (e.g., MERIS).